HHS Public Access

Author manuscript

J Control Release. Author manuscript; available in PMC 2016 September 10.

Published in final edited form as:

J Control Release. 2015 September 10; 213: 36–44. doi:10.1016/j.jconrel.2015.06.021.

SOD1 Nanozyme Salvages Ischemic Brain by Locally Protecting Cerebral Vasculature

Yuhang Jiang[1], **Anna M. Brynskikh, Ph.D.**[2], **Devika S-Manickam, Ph.D.**[1], and **Alexander V. Kabanov, PhD., Dr.Sc.**[2,3]

[1]Division of Molecular Pharmaceutics and Center for Nanomedicine in Drug Delivery, UNC Eshelman School of Pharmacy, University of North Carolina at Chapel Hill, Chapel Hill, NC 27599, USA

[2]Department of Pharmaceutical Sciences and Center for Drug Delivery and Nanomedicine, University of Nebraska Medical Center, Omaha, NE 68198, USA

[3]Laboratory for Chemical Design of Bionanomaterials, Faculty of Chemistry, M.V. Lomonosov Moscow State University, Moscow 117234, Russia

Abstract

Copper/zinc superoxide dismutase (CuZnSOD; SOD1) is widely considered as a potential therapeutic candidate for pathologies involving oxidative stress, but its application has been greatly hindered by delivery issues. In our previous study, nano-formulated SOD1 (*cl*-nanozyme) was shown to decrease infarct volume and improve sensorimotor functions after single intravenous (IV) injection in a rat middle cerebral artery occlusion (MCAO) model of ischemia/reperfusion (I/R) injury. However, it remained unclear how *cl*-nanozyme was able to deliver SOD1 to the brain and exert therapeutic efficacy. Present study aims to answer this question by exploring micro-distribution pattern of *cl*-nanozyme in the rat brain after stroke. Immunohistochemistry studies demonstrated *cl*-nanozyme co-localization with fibrin along damaged arteries and capillaries in the ischemic hemisphere. We further found that *cl*-nanozyme can be cross-linked into thrombi formed after I/R injury in the brain, and this effect is independent of animal species (rat/mouse) used for modeling I/R injury. This work is also the first report reinforcing therapeutic potential of *cl*-nanozyme in a well-characterized mouse MCAO model of I/R injury.

Graphical abstract

Correspondence: Dr. Alexander V. Kabanov and Dr. Devika S-Manickam, Division of Molecular Pharmaceutics and Center for Drug Delivery and Nanomedicine, UNC Eshelman School of Pharmacy, University of North Carolina at Chapel Hill, Chapel Hill, NC 27599, USA. kabanov@email.unc.edu; Phone: +1 (919) 537-3800; Fax: +1 (919) 962-9922. dsmanickam@unc.edu; Phone: +1 (919) 962-4654; Fax: +1 (919) 962-9922.

Disclosure/conflict of interest The authors declare no conflict of interest.

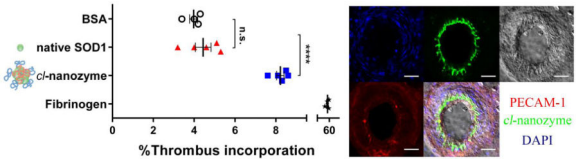

Keywords

stroke; superoxide dismutase; thrombus; blood-brain barrier; neurovascular unit; passive targeting

Introduction

Stroke affects 7 million people, and continues to kill over a hundred thousand people annually in the United States alone [1]. Main causes of brain tissue damage during transient ischemic stroke are ischemic and reperfusion injuries. Ischemic injury results from lack of glucose and oxygen when blood flow to the brain is blocked [2]. Reperfusion injury results from the detrimental action of reactive oxygen species (ROS) on brain tissue after blood flow is restored [3].

Antioxidant enzymes are endogenous tools for cells to scavenge ROS. However, their expression is often inhibited during stroke [4, 5], rendering antioxidant activity far less than sufficient for complete removal of excess ROS. Therefore, supplementation of antioxidant enzymes to the brain is a potential therapeutic strategy for this disease [6]. Their action would be especially beneficial for rescuing the salvageable penumbra since oxidative stress is the main mechanism of tissue damage in this area [7]. A direct use of anti-oxidant enzymes as therapy for stroke is not plausible because of its short half-life in the blood and poor permeability across the blood-brain barrier (BBB) and cellular membranes [8]. Even though BBB can be partially compromised during and after stroke, it still remains the key impediment for CNS transport of enzymes [9, 10]. Multiple strategies have been explored for delivery of functional antioxidant enzymes to the brain, including cationic liposomes, fusion proteins with peptide transduction domains, poly(ethyelene glycol)-protein conjugates (PEGylated protein) and encapsulation into poly(lactic-co-glycolic acid) (PLGA) nanoparticles [11–18]. However, each of these approaches has limitations that precluded their successful clinical use as discussed in our previous work [19]. Briefly, loading of enzymes into solid or hollow nanoparticles often resulted in loss of activity and/or unsatisfactory loading efficiency (32% in the case of SOD1 liposomes [20]), and PEGylation usually decreases enzyme permeability across BBB [13].

We have demonstrated a different approach for encapsulation and delivery of antioxidant enzymes to the brain [19, 21, 22]. This approach is based on incorporation of an antioxidant enzyme, such as SOD1, into nano-sized polyion complexes with cationic block copolymers (“nanozymes”). Nanozymes are core-shell structured nanoparticles with the polyion complex core consisting of charge-neutralized polycation chains and protein globules, and the shell consisting of PEG chains. Primary amine groups in the core were cross-linked (*cl*) using low molecular mass chemical cross-linkers to form *cl*-nanozyme and further purified to improve sample homogeneity by removing non-*cl*-nanozymes [19]. This formulation is

essentially a covalently cross-linked polyion complex formed by SOD1 and methoxy-poly(ethylene glycol)-b-poly(l-lysine) (PEG-pLL, Figure S1). Some of the key advantages of this strategy include high (100%) loading efficiency (owing to the formation of stoichiometric complexes) and instantaneous enzyme availability for catalysis precluding the need for its release, since superoxide anions are small enough to freely diffuse into the enzymatic core of the particle. This is a distinct advantage in scavenging ROS in the acute phase of diseases caused by oxidative stress, because the time window for antioxidant enzymes to work in these scenarios are usually narrow, and "fast acting" formulations like *cl*-nanozyme are consequently favored over those requiring drug release mechanisms.

The initial *in vivo* proof of concept for nanozyme transport to CNS was obtained by us using *cl*-nanozymes carrying butyrylcholinesterase, SOD1, or catalase [22, 23]. Compared to PEGylated SOD1 which poorly enters cells, SOD1 nanozyme was transported into neuronal cells and was superior to PEGylated SOD in depleting intracellular ROS and inhibiting Angiotensin II signaling *in vitro* and *in vivo* [24, 25]. Catalase nanozymes demonstrated neuroprotective effects in an animal model of Parkinson's disease (PD) [26, 27]. Our most recent results demonstrated the therapeutic efficacy of purified SOD1 *cl*-nanozyme in a rat middle cerebral artery occlusion (MCAO) model of I/R injury [19] by decreasing infarct volume and improving sensorimotor functions after a single IV bolus. Similar to other reports using nano-formulated SOD1 for the treatment of stroke [15, 18], we did not specifically investigate how this approach was able to exert the observed therapeutic effect [19]. However, understanding this mechanism can be essential for improving therapeutic potential of SOD1 nanozyme formulation and for discovery of more applications of the nanozyme delivery platform.

In the present work, we demonstrate that *cl*-nanozyme accumulated predominantly within the injured vasculature and co-localized with fibrin after stroke. This suggests one possible mechanism where *cl*-nanozyme passively target to damaged brain vasculature, and locally protect the neurovascular unit as an entire entity. To evaluate this finding from a translational perspective and investigate the validity of our findings in another animal model, we tested the same *cl*-nanozyme formulation in a well-characterized mouse model of stroke, and again observed significant reduction of infarct size. *In vitro* thrombus incorporation assay in the mouse plasma further supported our major hypothesis that *cl*-nanozyme can be actively incorporated into growing thrombus formed during or after stroke.

Materials and Methods

Materials

3,3'-Diaminobenzidine (DAB), SOD1, and 2,3,5-triphenyltetrazolium chloride (TTC) were purchased from Sigma-Aldrich. PEG_{113}-pLL_{51} was purchased from Alamanda Polymers™; Bovine serum albumin (BSA), ethanol, ethylenediaminetetraacetic acid (EDTA), 3,3´-dithiobis(sulfosuccinimidylpropionate) (DTSSP), 10% neutral buffered formalin, trichloroacetic acid (TCA) were purchased from Thermo Fisher Scientific. AlexaFluor® secondary antibodies, and Hoechst 43580 were purchased from Life Technologies; C57BL/6 mouse plasma was purchased from Molecular Innovations. All reagents and chemicals were used as received.

Animals

Charles River Laboratories supplied 8-week-old male Sprague-Dawley rats (250–300 g), and 12-week-old male C57BL/6 mice (20–28 g). Animals were housed and humanely handled in accordance with the Principles of Animal Care outlined by National Institutes of Health. They were allowed free access to food and water and were maintained under temperature, humidity, and light-controlled conditions. Institutional Animal Care and Use Committees (IACUC) of University of Nebraska Medical Center (UNMC) and the University of North Carolina at Chapel Hill approved all experiments involving animal subjects.

MCAO model of transient ischemic stroke in rats

Brain ischemia was modeled by transient MCAO method as described previously [28]. Rats were anesthetized with ketamine (80 mg/kg) and xylazine (5 mg/kg) cocktail and isoflurane (5% v/v for induction and 0.5% v/v during surgery). Rectal temperature was maintained at about 37 °C throughout the surgery using a homeothermic monitor (Harvard Apparatus, UK). Animals were prepared for surgery according to IACUC recommendations. The right common carotid artery was exposed and occluded using a silicon rubber-coated monofilament for MCAO. Filament was inserted through the incision into internal carotid artery (ICA) and further until reaching the bifurcation of MCA. Tip occluded the entrance to MCA and blocked blood supply to part of the right brain hemisphere (referred to as the ischemic hemisphere). Filament was carefully withdrawn after 1 hour. Sham surgery was performed as described above without filament insertion. After the surgery, animals were returned to their cages and allowed free access to water and food. At the time of reperfusion, 10,000 U/ kg of native SOD1 or *cl*-nanozyme (n = 10 in each group) were IV injected under anesthesia. Rats were sacrificed 3 or 24 h post-reperfusion, and perfused with 4% paraformaldehyde solution for histology analysis.

Histology and Immunohistochemistry

Tissue toxicity of *cl*-nanozyme was assessed by hematoxylin and eosin (H&E) staining of liver, spleen, kidney, and lung tissues. Tissue samples were dissected and fixed in 10% neutral buffered formalin before embedded in paraffin. Five μm thick tissue sections were processed and stained according to standard protocol used by Tissue Sciences core facility at UNMC. *Cl*-nanozymes were visualized in peripheral organs using DAB. Tissue samples were prepared as described above. For detection of *cl*-nanozyme in liver, spleen, kidney, and lung, respective tissue sections were incubated at 4 °C overnight with rabbit anti-PEG antibody (1:500, Abcam, MA), followed by incubation with secondary biotinylated goat anti-mouse antibodies and VecStain Elite kit (Vector Laboratories, CA). DAB color generation system was used as described previously [29] for chromogenic visualization. Fluorescent immunohistochemistry study was performed on tissues perfused with PBS followed by 10% neutral buffered formalin. To visualize *cl*-nanozyme in the liver and brain, tissue sections were stained using rabbit anti-PEG antibody (Abcam, CA) diluted 1:200 and 1:100, respectively. Hepatocytes were detected with polyclonal chicken anti-albumin antibody (1:100, Sigma Aldrich, MO). $CD68^+$ cells in the brain (infiltrating monocytes), liver (Kupffer cells) and spleen (splenic macrophages) were visualized using monoclonal

mouse anti-CD68 antibody (1:40 Abcam, MA). Brain microvessels were visualized using monoclonal mouse anti-CD31 antibody (1:30, AbD Serotec, NC); neurons were visualized using monoclonal mouse anti-neurofilament 70kDa (NF-L) antibody (1:200, Millipore, CA); fibrin deposits after stroke were visualized using mouse anti-fibrin antibody (1:50, Abcam, MA). Treatment with primary antibodies was followed by treatment with secondary antibodies: AlexaFluor 594 goat anti-chicken, AlexaFluor 594 goat anti-mouse, and AlexaFluor 488 goat anti-rabbit, and AlexaFluor 647 goat anti-mouse. Nuclei were visualized using 2.5μg/ml Hoechst 43580 solution. Immunofluorescence were detected using Zeiss 710 Confocal Laser Scanning Microscope and images were analyzed using Zeiss Zen software and ImageJ software (National Institute of Health, MD).

Preparation of ^{125}I-labeled Proteins and *Cl*-nanozyme

Native SOD1, fibrinogen, BSA, or *cl*-nanozyme were radioactively labeled with ^{125}I using chloramine-T method as previously described [30]. Briefly, 5 μg of protein or equivalent amount of *cl*-nanozyme was mixed with 0.5 mCi Na^{125}I (PerkinElmer, MA) in a final volume of 40 μL in sodium phosphate buffer (0.25 M, pH=7.5). Five μL freshly-made chloramine-T solution (2 μg/μL in sodium phosphate buffer) was added to the mixture. After 60 s incubation under constant mixing, the ^{125}I-labeled samples were purified using Illustra NAP-5 desalting columns (GE Healthcare, NJ). Fractions were collected in Eppendorf tubes pretreated with 1% BSA in Lactated Ringer's solution (1% BSA-LR) to prevent non-specific adsorbance. Radioactivity was measured using a PerkinElmer γ-counter. TCA precipitation was conducted to determine the ^{125}I association of labeled samples. Briefly, 1 μL of collected fractions was added to 0.5 mL of 1% BSA-LR and then precipitated in 0.5 mL of 30% TCA followed by centrifugation at 5000 ×g for 10 min at 4 °C. The resulting supernatant and pellet were measured in the γ-counter and the values were used to calculate the %radioactivity that precipitated with acid (% protein bound-^{125}I = [CPM_{pellet} /(CPM_{pellet} + $CPM_{supernatant}$)]*100%). Samples containing >100,000 cpm/μL of radioactivity and > 90% TCA precipitation were used for animal studies.

Biodistribution and Serum Clearance in Mice

Twelve-week-old male C57BL/6 mice were anesthetized by intraperitoneal (IP) injection of 0.2 mL of urethane (4.0 g/kg). Approximately 500,000 CPM of radiolabeled samples were injected IV via the jugular vein with 0.2 mL of 1% BSA-LR. For the biodistribution study, the abdomen and rib cage were opened and venous blood was collected by cardiac puncture 1 hour post-injection. Then, 20 mL of PBS was perfused through the left ventricle of the heart. At the end of study, organs were dissected and wet-weighed. For the serum clearance study, blood from the pre-exposed carotid artery was collected at various time points after injection. Serum was separated from whole blood by centrifugation at 5400 ×g for 10 min at 4 °C. Levels of radioactivity were measured in the γ-counter. To calculate serum clearance, the level of radioactivity was expressed relative to the amount injected (%Inj/mL) and these values were plotted against time (min) to construct the serum concentration vs. time curve.

MCAO Model of Transient Ischemic Stroke in Mice

All mice were randomly assigned before surgery into one of the following groups: *cl*-nanozyme-treated group (n = 8), native SOD1-treated group (n = 8), or saline-treated group (n = 7). The mice were weighed and were subjected to 90 min of ischemia under isoflurane anesthesia (5% v/v for induction and 1.5% v/v during surgery) as previously described [31]. Briefly, rectal temperature was monitored maintained at approximately 37 °C during surgery using a homothermic heating system. A midline ventral neck incision was made, and unilateral MCAO was performed by inserting a silicone rubber coated monofilament into the right internal carotid artery 6 mm from the internal carotid/pterygopalatine artery bifurcation via an external carotid artery stump. At the time of reperfusion, 10,000 U/ kg of treatment solutions were IV injected under anesthesia.

TTC Staining and Brain Infarct Volume Quantification

After 90 minutes of ischemia and 24 hours of reperfusion, the mice were euthanized and the brains were chilled at −80 °C for 4 minutes to slightly harden the tissue. Five 2-mm-thick coronal sections were cut from the olfactory bulb to the cerebellum and then stained with 1.5% TTC in PBS (pH=7.4). The sections in TTC solution were incubated in a water bath maintained at 37 °C for 30 minutes, then transferred to a 10% phosphate-buffered formalin solution and incubated overnight at 4 °C before pictures were taken for analysis. The infarct volumes were calculated blinded to the treatment given, and the infarct size in each of the five slices was quantified using the Image J software. In addition to total hemisphere, the infarct areas were determined separately for cortex and caudoputamen in each slice. Then the infarct areas on each slice were summed up and multiplied by thickness to calculate infarct volumes. The infarct volumes were calculated using Swanson's method [32] and processed as % contralateral hemisphere to avoid mis-measurements secondary to edema.

Thrombus Incorporation Assay in Mouse Plasma

One hundred thousand CPM of ^{125}I-labeled fibrinogen, BSA, native SOD1, and *cl*-nanozyme were added into an Eppendorf tube containing 1 mL C57BL/6 mouse Lithium heparin-stabilized plasma (Innovative Research, MI). Half mg of protamine sulfate was then added to neutralize heparin and allow thrombus formation. The tube was incubated on a rotary-shaker for 24 h at 4 °C before centrifugation at 5000×g for 10 min. Serum was separated from the white thrombus at the bottom of the tube, and then subjected to TCA precipitation assay to correct for error caused by ^{125}I dissociation during incubation as described above. Percentage of samples sequestered in the thrombus compartment were calculated using the following formula: %Thrombus Incorporation = [$CPM_{thrombus}$ / ($CPM_{thrombus}$ + CPM_{serum})]*100%.

Statistical Analysis

The randomization code was broken in the mice stroke therapeutic efficacy study after acquiring all the data. Statistical analysis was done using Prism 5.0 software (GraphPad, CA). Unpaired Student's t-test was used for two groups, and one-way ANOVA followed by Tukey's multiple comparison test for groups of three and above. A minimum pvalue of 0.05

was estimated as the significance level. Results of all experiments are presented as mean ± standard error of the mean (SEM).

Results

C*l*-nanozyme Tissue Distribution in the Rat MCAO Model of I/R Injury

In our previous paper [19] reporting synthesis and purification of *cl*-nanozyme, we have demonstrated decreased infarct volume and improved sensorimotor functions after a single IV injection in a rat MCAO model. To gain insight into the mechanism of *cl*-nanozyme's therapeutic efficacy, we studied its micro-distribution in the same model. Immunohistochemistry (IHC) analysis revealed accumulation of *cl*-nanozyme primarily in the ipsilateral hemisphere in the area of infarct at 3h post-reperfusion. (Figure S2).

Cl-nanozyme localized primarily within blood vessels, as shown by fluorescent double staining for *cl*-nanozyme and endothelial marker PECAM-1 in Figure 1A. *Cl*-nanozyme staining outside the blood vessel in brain parenchyma was primarily seen in the infarct region of the ipsilateral hemisphere. *Cl*-nanozyme co-localized with neither neurons nor activated mononuclear phagocytes (Figure S2).

We further hypothesized that *cl*-nanozyme co-localize with damaged blood vessels, since its signal was most prominent in infarct regions. Evidence for this hypothesis is shown in Figure 2. During the MCAO procedure, occlusion is created by filament insertion into the lumen along the internal carotid artery. Figure 2A is a confocal micrograph of a coronal brain section across a portion of internal carotid artery where the filament tip was positioned (Figure 2D).

The filament tip had damaged the artery during filament insertion and/or occlusion, as suggested by discontinuous nuclear staining around the luminal side of the artery (Figure 2C), and *cl*-nanozyme co-localized with these damaged portions of the artery (Figure2B and 2C). No *cl*-nanozyme signal was observed in the contralateral hemisphere where the internal carotid artery was not damaged, as shown in dotted box, Figure 2B. In infarcted brain regions, *cl*-nanozyme co-localized with fibrin, a protein involved in blood clotting (Figure1B and 1C), which further supports our hypothesis that *cl*-nanozyme localizes in damaged blood vessels. Interestingly, while most *cl*-nanozyme signal co-localized with fibrin, not all capillaries with fibrin deposition sites showed *cl*-nanozyme accumulation (Figure 1C).

Peripheral organs were collected 24 hours after reperfusion, and histological examinations was performed to qualitatively study the disposition and any possible toxicity effects of *cl*-nanozyme. H&E-stained tissue sections did not reveal any sign of acute toxicity (Figure S3). Analysis of *cl*-nanozyme distribution in select peripheral organs confirmed its presence in the liver and spleen, but not in lungs or kidneys at this time point (Figure 3A). Triple fluorescent immunostaining of the liver tissue revealed co-localization of *cl*-nanozyme with hepatocytes and Kupffer cells (Figure 3B). We noticed intense *cl*-nanozyme staining in areas between two adjacent hepatocytes indicative of its deposition in the bile canaliculi, suggesting a potential clearance mechanism via bile excretion. In addition to their

intracellular accumulation in hepatocytes, *cl*-nanozymes were also observed in liver sinusoids.

Cl-nanozyme Biodistribution and Serum Clearance in Mice

We studied biodistribution of native SOD1 and *cl*-nanozyme in healthy C57/B6 mice to determine the effects of formulating SOD1 on its biodistribution. One hour after injection, *cl*-nanozyme was found to accumulate in liver and spleen in significantly higher amounts than native SOD1, displaying 25- and 38-fold increases, respectively (Figure 4A). Changes in SOD1 accumulation in most other peripheral organs including heart, lung, and spine were significant but less drastic (less than 4-fold increase) compared to liver and spleen. However, *cl*-nanozyme accumulation in kidney was reduced by more than half compared to native SOD1 (35.4% vs. 88.3%). Notably, the brain uptake of *cl*-nanozyme was 2-fold higher than native SOD1 (0.0809% vs. 0.0406%) in healthy mice.

First-order kinetics was observed in the early phase of clearance for both substances, demonstrated by the statistically significant relation between log(%Inj/mL) and time (Figure 4B). Serum half-life ($t_{1/2}$) of native SOD1 and *cl*-nanozyme was 10.3 min and 33.8 min respectively, suggesting prolonged SOD1 circulation after formulation.

Therapeutic Effect of *Cl*-nanozyme in Mouse MCAO Model of I/R Injury

Cl-nanozymes administered at the onset of reperfusion in a mouse MCAO model of I/R injury resulted in reduced infarct volumes compared to groups treated with saline or native SOD1. Significantly reduced infarct volume was observed in all three brain regions analyzed (cortex: 35.0±7.0%; caudoputamen: 13.0±4.7%; hemisphere: 28.1±5. 6%) compared to those injected with saline (cortex: 69.8±3.7%; caudoputamen: 73.7±6.0%; hemisphere: 61.5±6.8%) and native SOD1 (cortex: 59.3±7.7%; caudoputamen: 78.9±6.5%; hemisphere: 57.1±6.9%), as shown in Figure 5. The mean infarct volume was slightly lower in the native SOD1-treated group than in saline-treated group, albeit this difference was not statistically significant. Interestingly, the protective effect of *cl*-nanozyme appears to be stronger in the caudoputamen area than in the cortex or entire hemisphere.

Thrombus Incorporation Assay

To directly evaluate the ability of *cl*-nanozyme and native SOD1 to be incorporated into white thrombi, we performed an *in vitro* thrombus incorporation assay using mouse plasma. After 24 h incubation at 4 °C, incorporation of native SOD1 into the thrombi (4.4±0.4%) was not significantly different from that of the negative control, BSA. However, significantly more *cl*-nanozyme (8.2±0.2%) was sequestered in the thrombus compartment (Figure 6). Fibrinogen was used as a positive control and showed 52±4% accumulation in the thrombi.

Discussion

Cl-nanozyme for delivery of antioxidant enzymes has been successfully used by us previously for the treatment of multiple pathologies involving oxidative damage [19, 21, 24, 25, 33–35]. Specifically, its therapeutic effect in decreasing the infarct volume and

improving sensorimotor functions upon single IV injection in a rat stroke model was demonstrated in our laboratory [19]. The present study continues to explore the mechanism by which *cl*-nanozyme exerted therapeutic efficacy.

The structure of *cl*-nanozyme does not include a brain targeting moiety. Thus, we did not expect it to cross a healthy BBB. Initially we believed that *cl*-nanozymes could possibly enter the brain via the disrupted BBB, a well-characterized phenomenon after brain I/R injury [36–38]. To our surprise, despite the observed therapeutic efficacy in the stroke model, we did not observe substantial evidence of *cl*-nanozyme crossing the BBB. In the IHC experiments, we did observe a considerable amount of *cl*-nanozyme signal associated with the infarct region of the brain, where the BBB is supposed to be disrupted. However, the majority of the signal was not associated with neurons or activated macrophages, but trapped inside the lumen of blood vessels. Although by design, our study does not exclude the possibility of a small portion of *cl*-nanozyme crossing the BBB and exerting therapeutic effect, the hypothesis of thrombus accumulation is apparently more plausible based on our observations. It also serves better on explaining why *cl*-nanozyme shows much better therapeutic efficacy compared to native SOD1, which can be tricky to explain based solely on the BBB disruption theory.

Our thrombus incorporation hypothesis is derived from the chemical composition of *cl*-nanozyme, with its core structure being charge-neutralized pLL/SOD1 complex. The monomer of pLL, ε -lysine is capable of cross-linking into the thrombus by participating in biochemical reactions accompanying its formation [39]. Briefly, blood vessel damage activates platelets and initiates a cascade of tissue factor (TF) activation, which converts TFXIII to its active form, TFXIIIa. TFXIIIa is a transglutaminase which cross-links glutamine with the ε-amine group of lysine. Indeed, pLL has been proved to be a good substrate for transglutaminase and this reaction has been utilized to enzymatically produce pLL-protein conjugates [40]. Therefore it is not surprising to see this reaction occurring *in vivo*.

IHC data in the rat model strongly supported the thrombus incorporation hypothesis. *Cl*-nanozyme was detected primarily in the infarct region in association with endothelial cells of the damaged brain vasculature. Intense *cl*-nanozyme signal was observed only in areas surrounding the injured internal carotid artery, but not the healthy one in the contralateral hemisphere (Figure 2B), confirming the selective nature of the association between *cl*-nanozyme and damaged blood vessels. Evidence of *cl*-nanozyme and thrombus crosslinking was further supported by the co-localization of *cl*-nanozyme with fibrin, a major component in blood clots, in the capillaries of the infarct region.

Beyond the brain, we have also examined *cl*-nanozyme distribution in select peripheral organs. H&E data suggested that *cl*-nanozyme is not noticeably toxic after *in vivo* administration. This is a promising observation that supports further development of such nanoparticles for stroke therapy. IHC experiments found massive distribution of *cl*-nanozyme into liver and spleen. This is generally in agreement with the known function of these organs in clearing particulate matter. Interestingly, a closer look at the liver slices revealed distribution of *cl*-nanozyme not only in Kupffer cells, but also in tube-shaped

territories between two adjacent hepatocytes that resemble bile canaliculi. This particular staining pattern possibly indicates that *cl*-nanozyme is excreted through bile as part of its metabolic pathway. What we have detected in these structures is more likely to be metabolic products than intact *cl*-nanozymes, especially considering the time point of analysis (24 h after reperfusion) and the cleavable disulfide bond present in the cross-linker (DTSSP) used in this formulation. Notably, the rat liver has been reported to have rather high concentrations (10 mM) of reduced glutathione known to participate in disulfide reduction, which thereby may enhance degradation of the *cl*-nanozyme in the liver [19]. In addition to intra-hepatocyte accumulation, staining was also observed in the liver sinusoids. Considering the $t_{1/2}$ of *cl*-nanozyme (33.8 min in mouse), it is unlikely that level of *cl*-nanozyme in the blood is high at this time point, i.e. 24 h after administration. Presence of *cl*-nanozyme in liver sinusoids may result from pLL binding to liver tissue, possibly via the same mechanism by which they bind to damaged blood vessels in the brain, since most of the blood coagulation proteins are synthesized in the liver [41].

These results in the rat MCAO model indicate that the therapeutic effect of *cl*-nanozyme can be attributed to its specific accumulation into damaged blood vessels in the infarct region. In events where blood vessels were damaged, intrinsic mechanisms of thrombosis could take place and actively recruit *cl*-nanozyme into them, thereby effectively reducing oxidative stress generated at the vicinity of damaged sites. Such blood vessel damage could result either from mechanical force (filament damaging ICA) or I/R injury (endothelium damage), both occurring in the MCAO model of stroke and the latter can also take place after transient stroke suffered by human subjects [42]. Since this mechanism appears to be translatable to human patients, we moved forward and investigated utility of *cl*-nanozymes in a different species to determine if similar therapeutic outcomes can be achieved in the mouse model of I/R injury. Indeed, this work is the first report reinforcing therapeutic potential of *cl*-nanozyme in a well-characterized mouse MCAO model [43].

Before evaluating *cl*-nanozyme in the mice MCAO model, we first conducted a comprehensive study to determine *cl*-nanozyme biodistribution in the early phase (1h) after injection. Similar to the rat model, we observed significantly increased sequestration of *cl*-nanozyme in the liver and spleen compared to native SOD1. Reduced uptake of *cl*-nanozyme in the kidney compared to that of native SOD1 (32 kDa) is in general agreement with the known function of kidney (glomerular filtration) in clearing small molecules with a molecular mass cutoff of ~40 kDa. Tissue distribution of protein is generally increased after formulation in most other organs, including a significant 2-fold increase in the brain. This increase probably resulted from a combination of decreased kidney accumulation and increased serum half-life as shown in Figure 4B.

Remarkably, *cl*-nanozyme administration resulted in significant reduction of infarct size in the mouse MCAO model compared to the native SOD1 group reinforcing its therapeutic potential in a second rodent model. Formation of micro-thrombi in capillaries after MCAO surgery is a well-documented phenomenon in rodent MCAO models [42, 44, 45]. Specifically, Zhang and colleagues [46] reported fibrin deposition primarily in the sub-cortex region after acute ischemic stroke, which may explain why therapeutic effect of *cl*-nanozyme is more pronounced in the caudoputamen compared to the cortex. Therefore, we

speculate that the mechanism of action of *cl*-nanozyme involves local protection of cerebral vasculature. Since the damaged brain endothelium in I/R injury is a site of intense ROS production [47], retention of *cl*-nanozyme in the sites of vascular damage and thrombus formation can facilitate its ability to scavenge local ROS and to subsequently mitigate detrimental effects of ROS on vasculature.

From a translational research perspective, clinically, different factors can contribute to local thrombus formation during the reperfusion phase of focal cerebral ischemia, as described by Virchow's triad: reduction in cerebral blood flow, damage to the vessel wall, and hypercoagulability. These events can contribute to the occurrence of focal "no-reflow" phenomenon [48] and even thromboembolic complications in the sub-acute phase of ischemic stroke [49]. In our thrombus incorporation study, we clearly demonstrated that *cl*-nanozyme can be actively incorporated into thrombus during their growth. This experimental set up is a simplified model where only white thrombi are formed. It can be postulated that in the scenario of clinical stroke where body temperature, blood cells, and platelets are all contributing to thrombus formation, the rate and extent of *cl*-nanozyme incorporation into thrombus could be faster and greater. By exploiting the "no-reflow" phenomenon and by passively accumulating at the site of injured arteries and microvessels after reperfusion, it is not surprising that *cl*-nanozyme exerted better therapeutic outcomes than native SOD1. Furthermore, passive targeting to sites of thrombus formation may open avenues for the delivery of agents that protect the endothelium from negative side effects of thrombolytics such as recombinant tissue plasminogen activator (rt-PA).

Two key works reported the use of particulate carriers for the delivery of SOD1 to treat stroke. Reddy and Labhasetwar demonstrated a 65% decrease in infarct volume compared to saline-treated group when SOD1 encapsulated in PLGA nanoparticles (NPs) was delivered via intracarotid (IC) injection to a rat MCAO model of stroke [15]. Interestingly, they also showed increased accumulation of HRP-loaded NPs in the ischemic hemisphere compared to its non-ischemic counterpart similar to our observation on increased accumulation of *cl*-nanozyme in the ischemic hemisphere. The authors pointed out the need for further research to understand the mechanism of NP-mediated protection. Yun *et al*. also showed a 50–60% decrease in infarct volume when SOD1 was delivered (again via the IC route) using 3 different nanoparticle platforms (liposomal SOD1, Polybutylcyanoacrylate-SOD1 and PLGA-SOD1 particles) in a mouse MCAO model of stoke [18]. SOD1 was conjugated to the distal end ($mPEG_{2000}$-DSPE) of liposomes prepared using phosphatidylcholine, cholesterol, mPEG2000-DSPE, and MAL-PEG2000-DSPE (molar ratio of 55:39:4:2). These carriers were modified with anti-NMDA receptor antibodies for brain targeting, and was shown to protect the ischemic regions by suppressing caspase-3 activation.

Although the present study is not unique in exploring therapeutic effect of SOD1 nano-formulations, it draws attention to the delivery of therapeutics to the neurovascular unit as a whole and in particular to the damaged brain endothelium, rather than neurons alone. Often researchers focus extensively on the delivery of therapeutics across the BBB to the brain parenchyma, a task that remains a formidable challenge in most cases. However, it can be not as formidable to target therapeutics to the BBB itself. Indeed, homeostatic interactions exist between endothelium and cerebral parenchyma, and the BBB has been considered to

be neuro-protective on its own by excreting neurotrophic factors in response to injury [50]. Our observations document that *cl*-nanozyme accumulates into damaged brain vasculature regions and probably exerts its effect mainly on brain vasculature rather than the parenchyma. It provides evidence that targeting therapeutics to the BBB itself could also be a viable therapeutic strategy. Another advantage of our approach is the use of IV administration route, which can be more desirable than IC from a translational perspective. This is made possible collaboratively by increased serum half-life and additional local retention at the damaged sites of vasculature. Moreover, our approach of drug administration after ischemic episode, as opposed to pretreatment with SOD1 formulations, as reviewed by Margaill *et al*.[6], is advantageous from translational standpoint as well.

Conclusion

In conclusion, the present study demonstrates the ability of *cl*-nanozyme to accumulate in damaged blood vessels. This allowed therapeutic cargo to exert its effect at the interface of blood and brain especially vulnerable to oxidative stress in stroke. We believe that *cl*-nanozyme is a promising delivery strategy that can find application in the therapy of cerebrovascular conditions associated with oxidative stress and inflammation. Evaluation of *cl*-nanozyme safety and efficacy in alternate models of transient ischemic stroke, e.g. MCAO procedure conducted on aged animals and/or animals with co-morbidities, is essential for further validation of the translational potential of this work.

Supplementary Material

Refer to Web version on PubMed Central for supplementary material.

Acknowledgements

We thank Dr. Louise D. McCullough (University of Connecticut Health Center) and members of her laboratory for mice MCAO procedure training and valuable suggestions; Dr. Hong Yuan (University of North Carolina at Chapel Hill; UNC-CH) for helpful discussions on stroke pathology and experimental design; Dr. Xiang Yi (UNC-CH) and Dr. William Banks (University of Washington, WA) for training and advice regarding iodination of SOD1 *cl*-nanozyme; Drs. Michael Jay and Zibo Li (UNC-CH) for sharing and helping with gamma counters in radioactivity assays; Dr. Robert Bagnell (UNC Microscope services laboratory) for assistance with confocal microscopy; UNMC Tissue Sciences facility and UNC's Lineberger Comprehensive Cancer Center, the Animal Histopathology Core Facility for their help with tissue sectioning and processing, and Mr. Nazar Filonov (Nanomedicines Characterization Core Facility, UNC-CH) for help with ICP-MS analysis.

This work was supported by the National Institutes of Health grant RO1NS051334, Institutional Development Award (IDeA) from the National Institute of General Medical Sciences of the National Institutes of Health under grant P20GM103480, as well as *The Carolina Partnership*, a strategic partnership between the UNC Eshelman School of Pharmacy and The University Cancer Research Fund through the Lineberger Comprehensive Cancer Center.

Reference

1. Lloyd-Jones. Heart Disease and Stroke Statistics-2009 Update: A Report From the American Heart Association Statistics Committee and Stroke Statistics Subcommittee (vol 119, pg e21, 2009). Circulation. 2010; 122:E11–E11.
2. Hinkle JL, Guanci MM. Acute ischemic stroke review. The Journal of neuroscience nursing : journal of the American Association of Neuroscience Nurses. 2007; 39:285–293. 310. [PubMed: 17966295]

3. Rodrigo R, Fernandez-Gajardo R, Gutierrez R, Matamala JM, Carrasco R, Miranda-Merchak A, Feuerhake W. Oxidative Stress and Pathophysiology of Ischemic Stroke: Novel Therapeutic Opportunities. Cns Neurol Disord-Dr. 2013; 12:698–714.
4. Spranger M, Krempien S, Schwab S, Donneberg S, Hacke W. Superoxide dismutase activity in serum of patients with acute cerebral ischemic injury - Correlation with clinical course and infarct size. Stroke. 1997; 28:2425–2428. [PubMed: 9412626]
5. Jung JE, Kim GS, Narasimhan P, Song YS, Chan PH. Regulation of Mn-Superoxide Dismutase Activity and Neuroprotection by STAT3 in Mice after Cerebral Ischemia. Journal of Neuroscience. 2009; 29:7003–7014. [PubMed: 19474327]
6. Margaill I, Plotkine M, Lerouet D. Antioxidant strategies in the treatment of stroke. Free Radic Biol Med. 2005; 39:429–443. [PubMed: 16043015]
7. Hughes JL, Beech JS, Jones PS, Wang D, Menon DK, Baron JC. Mapping selective neuronal loss and microglial activation in the salvaged neocortical penumbra in the rat. Neuroimage. 2010; 49:19–31. [PubMed: 19716426]
8. Banks WA. Delivery of peptides to the brain: Emphasis on therapeutic development. Biopolymers. 2008; 90:589–594. [PubMed: 18335425]
9. Sood R, Yang Y, Taheri S, Candelario-Jalil E, Estrada EY, Walker EJ, Thompson J, Rosenberg GA. Increased apparent diffusion coefficients on MRI linked with matrix metalloproteinases and edema in white matter after bilateral carotid artery occlusion in rats. J Cerebr Blood F Met. 2009; 29:308–316.
10. Zhang Y, Pardridge WM. Conjugation of brain-derived neurotrophic factor to a blood-brain barrier drug targeting system enables neuroprotection in regional brain ischemia following intravenous injection of tbe neurotrophin. Brain research. 2001; 889:49–56. [PubMed: 11166685]
11. Eum WS, Kim DW, Hwang IK, Yoo KY, Kang TC, Jang SH, Choi HS, Choi SH, Kim YH, Kim SY, Kwon HY, Kang JH, Kwon OS, Cho SW, Le KS, Park J, Won MH, Choi SY. In vivo protein transduction: biologically active intact pep-1-superoxide dismutase fusion protein efficiently protects against ischemic insult (vol 37, pg 1656, 2004). Free Radical Bio Med. 2005; 38:406–406.
12. Kim DW, Jeong HJ, Kang HW, Shin MJ, Sohn EJ, Kim MJ, Ahn EH, An JJ, Jang SH, Yoo KY, Won MH, Kang TC, Hwang IK, Kwon OS, Cho SW, Park J, Eum WS, Choi SY. Transduced human PEP-1-catalase fusion protein attenuates ischemic neuronal damage. Free Radical Bio Med. 2009; 47:941–952. [PubMed: 19577641]
13. Veronese FM, Caliceti P, Schiavon O, Sergi M. Polyethylene glycol-superoxide dismutase, a conjugate in search of exploitation. Adv Drug Deliver Rev. 2002; 54:587–606.
14. Francis JW, Ren JM, Warren L, Brown RH, Finklestein SP. Postischemic infusion of Cu/Zn superoxide dismutase or SOD:Tet451 reduces cerebral infarction following focal ischemia/reperfusion in rats. Exp Neurol. 1997; 146:435–443. [PubMed: 9270054]
15. Reddy MK, Labhasetwar V. Nanoparticle-mediated delivery of superoxide dismutase to the brain: an effective strategy to reduce ischemia-reperfusion injury. Faseb Journal. 2009; 23:1384–1395. [PubMed: 19124559]
16. Chan PH, Longar S, Fishman RA. Protective Effects of Liposome-Entrapped Superoxide-Dismutase on Posttraumatic Brain Edema. Ann Neurol. 1987; 21:540–547. [PubMed: 3037989]
17. Imaizumi S, Woolworth V, Fishman RA, Chan PH. Liposome-Entrapped Superoxide- Dismutase Reduces Cerebral Infarction in Cerebral-Ischemia in Rats. Stroke. 1990; 21:1312–1317. [PubMed: 2396268]
18. Yun X, Maximov VD, Yu J, Zhu H, Vertegel AA, Kindy MS. Nanoparticles for targeted delivery of antioxidant enzymes to the brain after cerebral ischemia and reperfusion injury. Journal of cerebral blood flow and metabolism : official journal of the International Society of Cerebral Blood Flow and Metabolism. 2013; 33:583–592.
19. Manickam DS, Brynskikh AM, Kopanic JL, Sorgen PL, Klyachko NL, Batrakova EV, Bronich TK, Kabanov AV. Well-defined cross-linked antioxidant nanozymes for treatment of ischemic brain injury. Journal of Controlled Release. 2012; 162:636–645. [PubMed: 22902590]
20. Yusa T, Crapo JD, Freeman BA. Liposome-mediated augmentation of brain SOD and catalase inhibits CNS O2 toxicity. Journal of applied physiology: respiratory, environmental and exercise physiology. 1984; 57:1674–1681.

21. Batrakova EV, Li S, Reynolds AD, Mosley RL, Bronich TK, Kabanov AV, Gendelman HE. A Macrophage-Nanozyme Delivery System for Parkinson's Disease. Bioconjugate Chemistry. 2007; 18:1498–1506. [PubMed: 17760417]
22. Klyachko NL, Manickam DS, Brynskikh AM, Uglanova SV, Li S, Higginbotham SM, Bronich TK, Batrakova EV, Kabanov AV. Cross-linked antioxidant nanozymes for improved delivery to CNS. Nanomedicine : nanotechnology, biology, and medicine. 2012; 8:119–129.
23. Gaydess A, Duysen E, Li YA, Gilman V, Kabanov A, Lockridge O, Bronich T. Visualization of exogenous delivery of nanoformulated butyrylcholinesterase to the central nervous system. Chem-Biol Interact. 2010; 187:295–298. [PubMed: 20060815]
24. Rosenbaugh EG, Roat JW, Gao L, Yang RF, Manickam DS, Yin JX, Schultz HD, Bronich TK, Batrakova EV, Kabanov AV, Zucker IH, Zimmerman MC. The attenuation of central angiotensin II-dependent pressor response and intra-neuronal signaling by intracarotid injection of nanoformulated copper/zinc superoxide dismutase. Biomaterials. 2010; 31:5218–5226. [PubMed: 20378166]
25. Savalia K, Manickam DS, Rosenbaugh EG, Tian J, Ahmad IM, Kabanov AV, Zimmerman MC. Neuronal uptake of nanoformulated superoxide dismutase and attenuation of angiotensin II-dependent hypertension after central administration. Free radical biology & medicine. 2014; 73:299–307. [PubMed: 24924945]
26. Brynskikh AM, Zhao YL, Mosley RL, Li S, Boska MD, Klyachko NL, Kabanov AV, Gendelman HE, Batrakova EV. Macrophage delivery of therapeutic nanozymes in a murine model of Parkinson's disease. Nanomedicine : nanotechnology, biology, and medicine. 2010; 5:379–396.
27. Klyachko NL, Haney MJ, Zhao Y, Manickam DS, Mahajan V, Suresh P, Hingtgen SD, Mosley RL, Gendelman HE, Kabanov AV, Batrakova EV. Macrophages offer a paradigm switch for CNS delivery of therapeutic proteins. Nanomedicine (London, England). 2014; 9:1403–1422.
28. Longa EZ, Weinstein PR, Carlson S, Cummins R. Reversible middle cerebral artery occlusion without craniectomy in rats. Stroke; a journal of cerebral circulation. 1989; 20:84–91.
29. Tieu K, Perier C, Caspersen C, Teismann P, Wu D-C, Yan S-D, Naini A, Vila M, Jackson-Lewis V, Ramasamy R, Przedborski S. D-β-Hydroxybutyrate rescues mitochondrial respiration and mitigates features of Parkinson disease. The Journal of Clinical Investigation. 2003; 112:892–901. [PubMed: 12975474]
30. Price TO, Farr SA, Yi X, Vinogradov S, Batrakova E, Banks WA, Kabanov AV. Transport across the blood-brain barrier of pluronic leptin. The Journal of pharmacology and experimental therapeutics. 2010; 333:253–263. [PubMed: 20053933]
31. McCullough LD, Blizzard K, Simpson ER, Oz OK, Hurn PD. Aromatase cytochrome P450 and extragonadal estrogen play a role in ischemic neuroprotection. The Journal of neuroscience : the official journal of the Society for Neuroscience. 2003; 23:8701–8705. [PubMed: 14507969]
32. Swanson RA, Morton MT, Tsao-Wu G, Savalos RA, Davidson C, Sharp FR. A semiautomated method for measuring brain infarct volume. Journal of cerebral blood flow and metabolism : official journal of the International Society of Cerebral Blood Flow and Metabolism. 1990; 10:290–293.
33. Brynskikh AM, Zhao Y, Mosley RL, Li S, Boska MD, Klyachko NL, Kabanov AV, Gendelman HE, Batrakova EV. Macrophage delivery of therapeutic nanozymes in a murine model of Parkinson’s disease, nanomedicine (Lond.). 2010; 5:379–396.
34. Klyachko NL, Haney MJ, Zhao Y, Manickam DS, Mahajan V, Suresh P, Mosley RL, Gendelman HE, Kabanov A, Batrakova E. Macrophages Offer a Paradigm Switch for CNS Nanozyme Delivery. Nanomedicine Accepted. 2013
35. Rosenbaugh EG, Savalia KK, Manickam DS, Zimmerman MC. Antioxidant-based therapies for angiotensin II-associated cardiovascular diseases. American Journal of Physiology - Regulatory, Integrative and Comparative Physiology. 2013; 304:R917–R928.
36. Brown RC, Davis TP. Calcium modulation of adherens and tight junction function: a potential mechanism for blood-brain barrier disruption after stroke. Stroke. 2002; 33:1706–1711. [PubMed: 12053015]

37. Nagaraja TN, Keenan KA, Brown SL, Fenstermacher JD, Knight RA. Relative distribution of plasma flow markers and red blood cells across BBB openings in acute cerebral ischemia. Neurol Res. 2007; 29:78–80. [PubMed: 17427280]

38. Nagaraja TN, Keenan KA, Fenstermacher JD, Knight RA. Acute leakage patterns of fluorescent plasma flow markers after transient focal cerebral ischemia suggest large openings in blood-brain barrier. Microcirculation. 2008; 15:1–14. [PubMed: 17934962]

39. Richardson VR, Cordell P, Standeven KF, Carter AM. Substrates of Factor XIII-A: roles in thrombosis and wound healing. Clinical science. 2013; 124:123–137. [PubMed: 23075332]

40. Sala A, Ehrbar M, Trentin D, Schoenmakers RG, Voros J, Weber FE. Enzyme mediated site-specific surface modification. Langmuir : the ACS journal of surfaces and colloids. 2010; 26:11127–11134. [PubMed: 20545368]

41. Mammen EF. Coagulation abnormalities in liver disease. Hematology/oncology clinics of North America. 1992; 6:1247–1257. [PubMed: 1333467]

42. Heye N, Paetzold C, Steinberg R, Cervos-Navarro J. The topography of microthrombi in ischemic brain infarct. Acta neurologica Scandinavica. 1992; 86:450–454. [PubMed: 1481626]

43. Liu F, Schafer DP, McCullough LD. TTC, fluoro-Jade B and NeuN staining confirm evolving phases of infarction induced by middle cerebral artery occlusion. Journal of neuroscience methods. 2009; 179:1–8. [PubMed: 19167427]

44. Choudhri TF, Hoh BL, Zerwes HG, Prestigiacomo CJ, Kim SC, Connolly ES Jr, Kottirsch G, Pinsky DJ. Reduced microvascular thrombosis and improved outcome in acute murine stroke by inhibiting GP IIb/IIIa receptor-mediated platelet aggregation. The Journal of clinical investigation. 1998; 102:1301–1310. [PubMed: 9769322]

45. Stoll G, Kleinschnitz C, Nieswandt B. Molecular mechanisms of thrombus formation in ischemic stroke: novel insights and targets for treatment. Blood. 2008; 112:3555–3562. [PubMed: 18676880]

46. Zhang ZG, Chopp M, Goussev A, Lu DY, Morris D, Tsang W, Powers C, Ho KL. Cerebral microvascular obstruction by fibrin is associated with upregulation of PAI-1 acutely after onset of focal embolic ischemia in rats. Journal of Neuroscience. 1999; 19:10898–10907. [PubMed: 10594071]

47. Eltzschig HK, Collard CD. Vascular ischaemia and reperfusion injury. British medical bulletin. 2004; 70:71–86. [PubMed: 15494470]

48. del Zoppo GJ. Virchow's triad: the vascular basis of cerebral injury. Reviews in neurological diseases. 2008; 5(Suppl 1):S12–S21. [PubMed: 18645567]

49. Kelly J, Rudd A, Lewis RR, Coshall C, Moody A, Hunt BJ. Venous thromboembolism after acute ischemic stroke: a prospective study using magnetic resonance direct thrombus imaging. Stroke. 2004; 35:2320–2325. [PubMed: 15322298]

50. Guo S, Kim WJ, Lok J, Lee SR, Besancon E, Luo BH, Stins MF, Wang X, Dedhar S, Lo EH. Neuroprotection via matrix-trophic coupling between cerebral endothelial cells and neurons. Proceedings of the National Academy of Sciences of the United States of America. 2008; 105:7582–7587. [PubMed: 18495934]

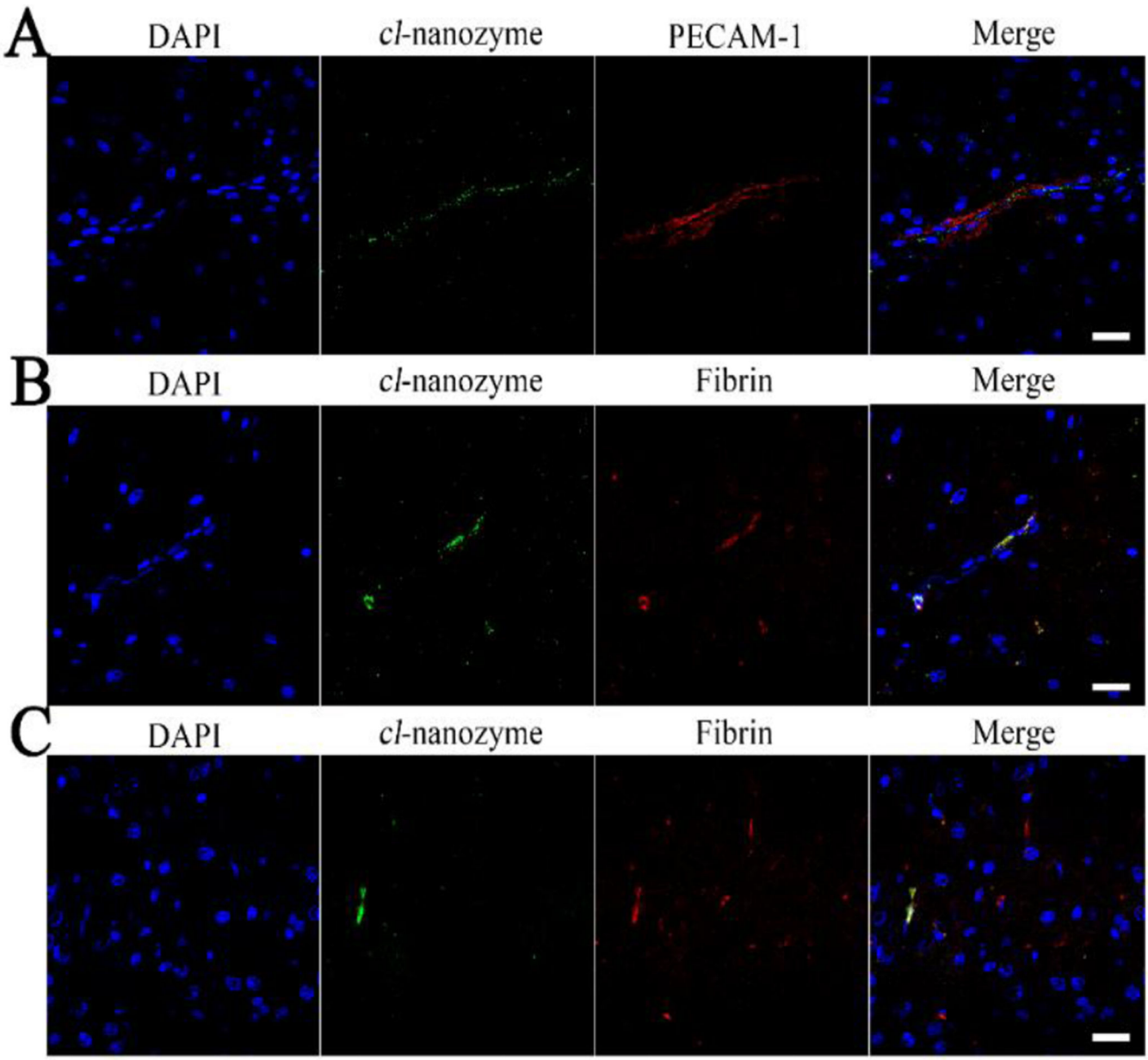

Figure 1. Distribution of *Cl*-nanozyme in the Rat Brain

Distribution of *cl*-nanozyme in the ipsilateral hemisphere of rat brains after I/R injury determined by immunofluorescence. **A.** *Cl*-nanozyme (PEG, green) was detected primarily in association with micro vessels (PECAM-1, red). **B.** Most *cl*-nanozyme signal co-localized with fibrin in rat brains after stroke, indicating possible interactions between *cl*-nanozyme and thrombus components. **C.** Not all fibrin signal in the brain were co-localized with *cl*-nanozyme. Nuclei are counterstained with DAPI, scale bars represent 20 μm.

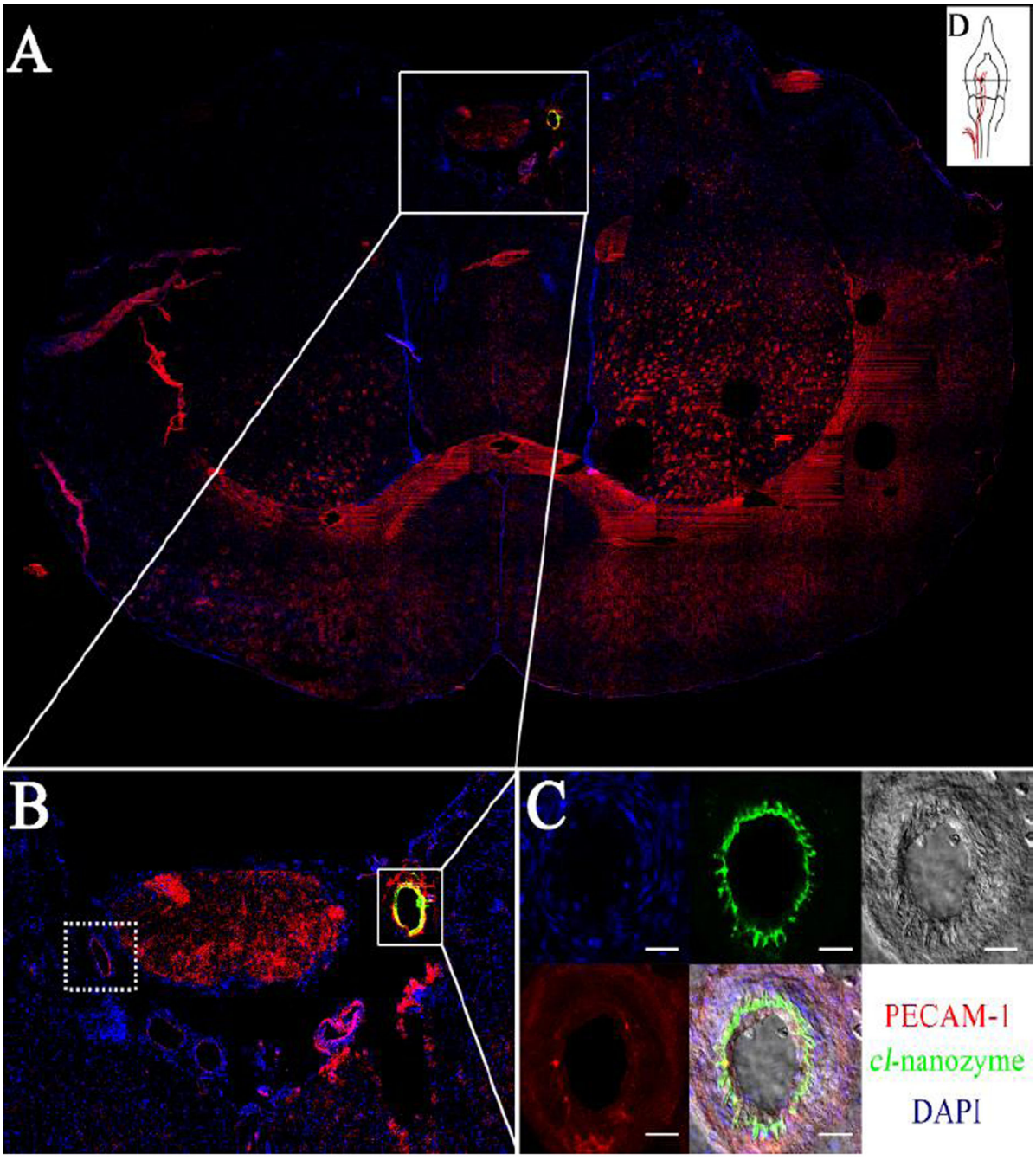

Figure 2. *Cl*-nanozyme Accumulation in the Damaged Internal Carotid Artery (ICA)

The ICA in the ipsilateral hemisphere in the rat brain showed intense staining for *cl*-nanozyme, which was not observed in the contralateral hemisphere. **A.** The ICA in the ipsilateral hemisphere was the only artery that showed very strong *cl*-nanozyme staining in the whole brain; **B.** 2.5× magnification of the squared area in A. Sub-arachnoid region shows that this staining was present only in the ipsilateral hemisphere, but not in the contralateral hemisphere; **C.** Confocal image of this artery shows *cl*-nanozyme co-localization with the injured endothelium cells lining the internal surface of this artery. Scale

bars represent 20 μm. **D.** A graphic illustration of the position of the brain section shown in **A**.

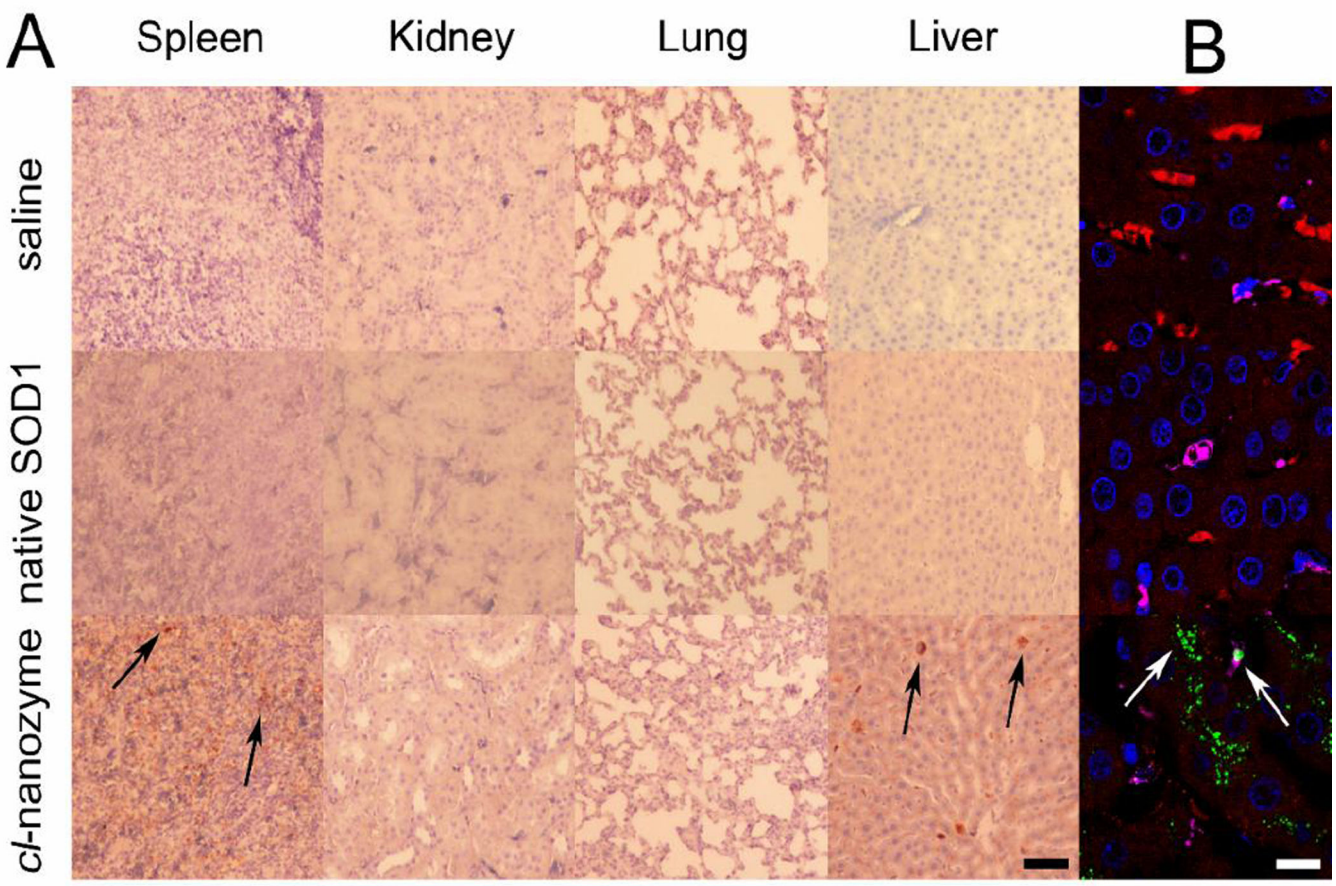

Figure 3. Distribution of *Cl*-nanozyme in Rat Peripheral Organs

Representative bright field micrographs of tissue sections harvested from MCAO rats 24 h after reperfusion. DAB was used to visualize *cl*-nanozyme in the tissue sections (black arrows). Scale bar represents 50 μm. **B.** Representative confocal fluorescent micrograph of liver tissue sections harvested from stroke rats 24 h after reperfusion and *cl*-nanozyme administration. Fluorescent immunohistochemistry demonstrated *cl*-nanozyme micro-distribution within the liver: red – hepatocytes; pink - Kupffer cells; green – *cl*-nanozyme; blue – nuclei. Scale bar represents 10 μm. Treatment groups are the same as shown in **A**.

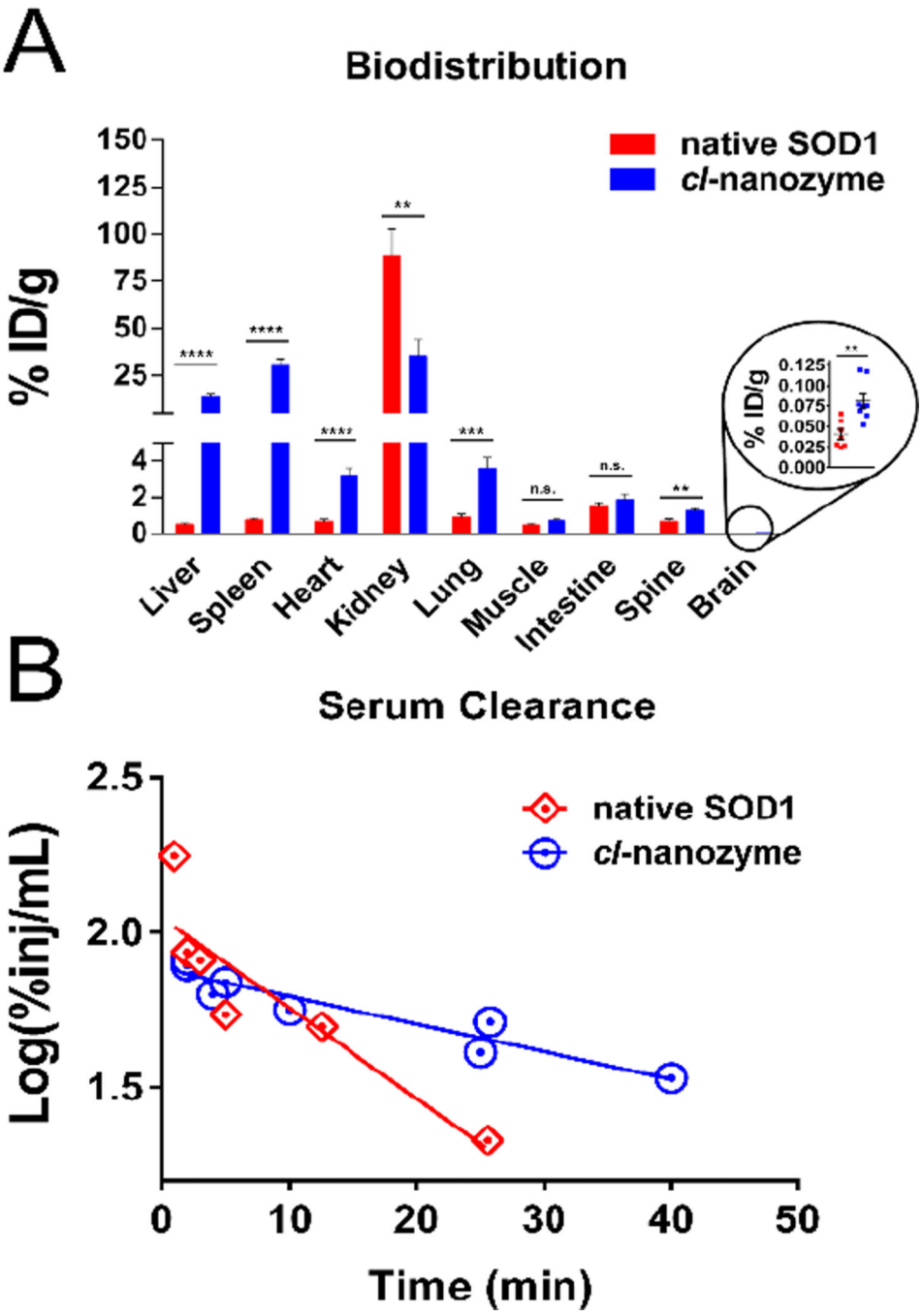

Figure 4. Biodistribution and Serum Clearance of Native SOD1 and *Cl*-nanozyme in healthy mice

A. C57BL/6 mice received IV bolus injection of either ^{125}I-labeled native SOD1 (n=7), or *cl*-nanozyme (n=8). One hour later organs were harvested and radioactivity was measured. Results represent mean % of injected dose per gram of tissue (ID%/g) with error bars representing ±SEM. Statistical significance was determined by Student's t-test (indicated as follows: n.s., not significant; *, P<0.05; **, P<0.01; ***, P<0.001; ****, P<0.0001); B. Serum clearance profiles of native SOD1 and *cl*-nanozyme were plotted and analyzed by

linear regression fitting. The serum half-life was 33.8 min (R^2=8966, P<0.0005; n=1–2 mice/time point) for *cl*-nanozyme, and 10.3 min (R^2=8156, P<0.05; n=1–2 mice/time point) for native SOD1.

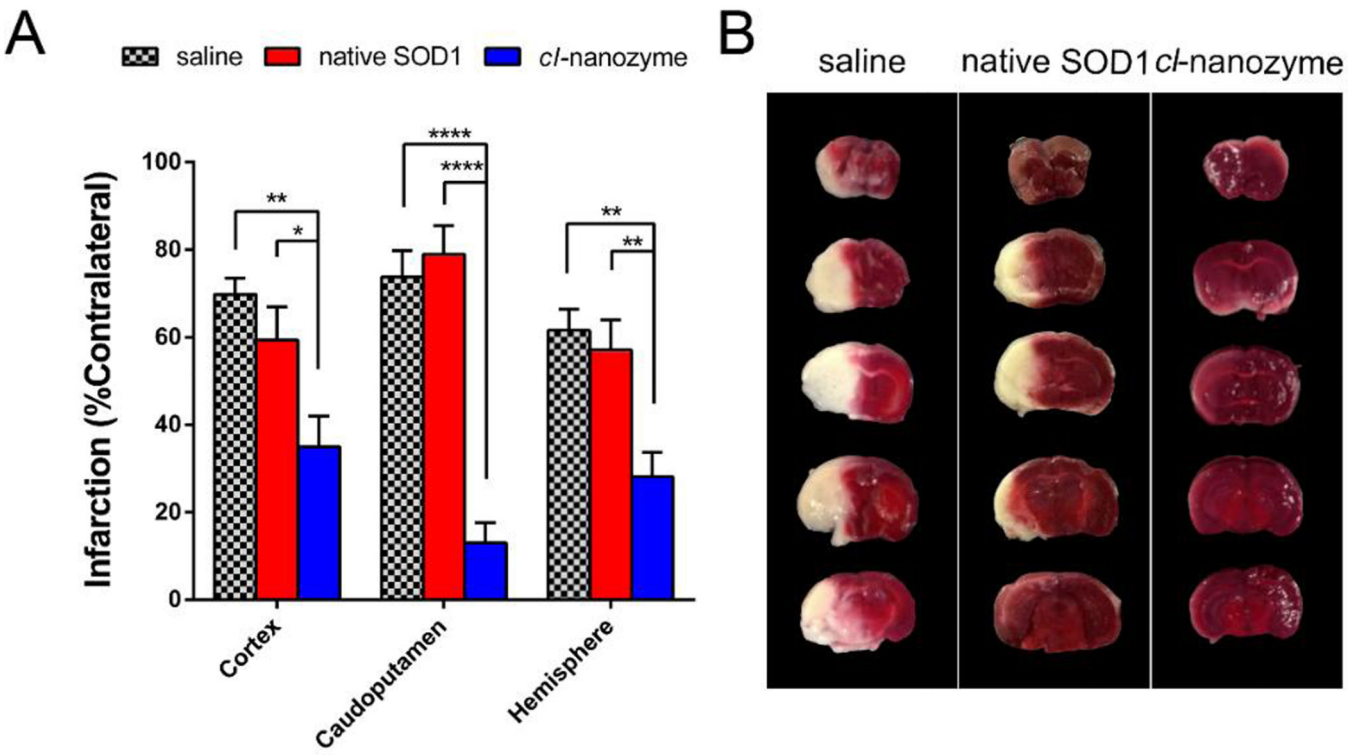

Figure 5. Therapeutic Efficacy of *Cl*-nanozyme in Mice MCAO Model of I/R Injury

At the onset of reperfusion, 10,000 U/kg of native SOD1 (n = 8), *cl*-nanozyme (n = 8), or equal volumes of saline (n = 7) were injected through the right jugular vein of the mice under anesthesia. Twenty-four hours after reperfusion, mice were euthanized and their brains were sectioned and stained using TTC solution. **A.** Bar graph showing infarct volume reduction. Infarction (% contralateral) was quantified as described in the methods section. Data were analyzed using one-way ANOVA with Tukey's post-hoc test and presented as mean ± SEM. Statistical significance is defined as $P<0.05$, and indicated by * ($P<0.05$), ** ($P<0.01$), or **** ($P<0.0001$). **B.** Representative coronal brain sections from animals receiving different treatments stained using TTC. Dark-colored areas indicate viable tissue; pale-colored areas indicate dead (infarcted) tissue.

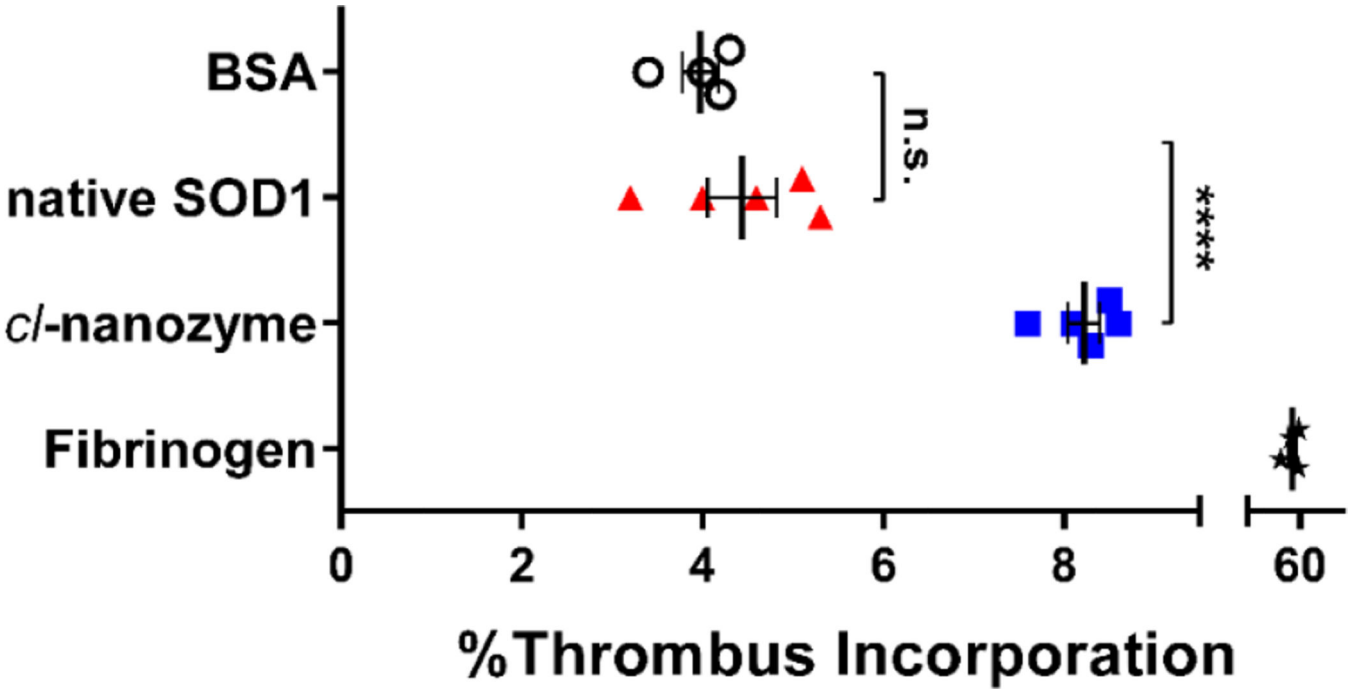

Figure 6. Thrombus Incorporation Assay in Mouse Plasma

Native SOD1 and *cl*-nanozyme were labeled using ^{125}I before incubation with mouse plasma for 24 h at 4 °C. The plasma was then centrifuged to separate thrombus and serum. The percentage of radioactivity in the thrombus compartment was calculated as described in the methods section. BSA and fibrinogen were also labeled and used in parallel as negative and positive controls. Data were analyzed using unpaired Student's t-test and are presented as mean ± SEM (n=4 or 5). Statistical significance is defined as $P<0.05$, and indicated by n.s. (not significant) or **** ($P<0.0001$).